RSC Publishing Journal of Materials Chemistry

Optical and Electrical Effects of Gold Nanoparticles in the active layer of Polymer Solar Cells

Journal:	*Journal of Materials Chemistry*
Manuscript ID:	JM-ART-08-2011-014150
Article Type:	Paper
Date Submitted by the Author:	24-Aug-2011

Complete List of Authors:	Wang, Charlie; the University of Hong Kong, Electrical and Electronic Engineering Choy, Wallace; the University of Hong Kong, Electrical and Electronic Engineering Duan, Chunhui; South China University of Technology, Institute of Polymer Optoelectronic Materials & Devices Fung, Dixon; The University of Hong Kong, eee Sha, Wei; the University of Hong Kong, Electrical and Electronic Engineering Xie, Fengxian; the University of Hong Kong, Electrical and Electronic Engineering Huang, Fei; South China University of Technology, Institute of Polymer Optoelectronic Materials & Devices Cao, Yong; South China University of Technology, Institute of Polymer Optoelectronic Materials & Devices

Journal of Materials Chemistry

Cite this: DOI: 10.1039/c0xx00000x

www.rsc.org/xxxxxx

Paper

Optical and Electrical Effects of Gold Nanoparticles in the active layer of Polymer Solar Cells

Charlie C. D. Wang[a], Wallace C. H. Choy[a]*, Chunhui Duan[b], Dixon D. S. Fung[a], Wei E.I. Sha[a], Feng-Xian Xie[a], Fei Huang[b]*, and Yong Cao[b]

Abstract

The effects of Au nanoparticles (NPs) incorporated into the active layer of polymer solar cells (PSCs) with a newly synthesized donor polymer are investigated in detail. Our work shows that localized surface plasmonic resonance (LSPR) introduced by the metallic NPs can experimentally and theoretically enhance the light absorption in the active layer of PSCs because the strong LSPR near field mainly distributes laterally along the active layer. The understanding can be applied to other metallic NPs incorporated organic solar cells. Meanwhile, our results show that electrical properties can counter-diminish the optical enhancement from LSPR and thus reduces the overall performance improvement. It is important that both optical and electrical properties need to be studied and optimized simultaneously for achieving improved power conversion efficiency. The study contributes to better understanding on the uses of Au NPs for enhancing PSC performances.

[a] *Department of Electrical and Electronic Engineering, University of Hong Kong, Pokfulam Road, Hong Kong, China. E-mail: chchoy@eee.hku.hk, Tel: (852)-2857-8485; Fax: (852)-2559-8738*

[b] *Institute of Polymer Optoelectronic Materials & Devices, State Key Laboratory of Physics and Chemistry of Luminescence, South China University of Technology, Guangzhou 510640, P. R. China, Email: msfhuang@scut.edu.cn, Tel: (86)-20-8711-4346*

† Electronic Supplementary Information (ESI) available, see DOI: 10.1039/b000000x/

Keywords: Gold nanoparticles, optical and electrical effects, surface plasmons, exciton dissociation, polymer solar cells

1. Introduction

Bulk heterojunction (BHJ) polymer solar cells (PSCs) are one of the very promising candidates for photovoltaic devices due to the efficient charge transfer from conjugated polymers to fullerene derivatives.[1,2] Compared with inorganic solar cells, however, one important hindrance for the efficiency improvement of PSCs is the limited light absorption due to the thin active layer limited by the short exciton diffusion length and low carrier mobility.[3-5]

Metallic nanoparticles (NPs) such as Au and Ag NPs and other metallic nanostructures can be potential candidates for improving the light absorption due to the localized surface plasmon resonance (LSPR) which contributes to the significant enhancement of local electromagnetic fields and thus improves the optical properties of the nanostructure devices.[6-11] In addition, the incident photons can be scattered for a longer propagation path in the active layer by metallic nanostructures.[6,12] These features can potentially benefit the light absorption and photocurrent generation of PSCs.

The incorporation of metallic NPs has been exploring in PSCs for improving photovoltaic performances.[13-18] However, the contributions of metallic NPs for improving PSC performances are still not conclusive. For instance, the enhancement of PSC photocurrent by incorporating metallic NPs has been demonstrated experimentally. The enhancement is commonly ascribed to LSPR excitation by using the improvement of incident photon-to-electron conversion efficiency (IPCE).[8,14,15] However, limitations exist in using IPCE as the evidence for LSPR effect because, apart from optical properties, IPCE is also highly affected by electrical properties such as exciton dissociation, hole and electron transport and collection at their respective electrodes.

In addition, many studies have used the metallic NPs as an interfacial layer on Indium tin oxide (ITO)-coated glass substrates or a dopant of buffer layers such as poly-(3,4-ethylenedioxythiophene)

:poly(styrenesulfonate) (PEDOT:PSS).[8,13-16] PSCs with the incorporation of metallic NPs into the active layer, however, have received limited investigation.[17-19] Therefore, the study for further understanding both optical and electrical properties is highly desirable for PSCs with metallic NPs incorporated into the active layer.

In this work, we will demonstrate the impact of the incorporation of monofunctional poly(ethylene glycol) (PEG)-capped Au NPs into the active layer of polymer blend. A newly synthesized polymer poly[2,7-(9,9-dioctylfluorene)-*alt*-2-((4-(diphenylamino) phenyl)thiophen-2-yl)malononitrile] (PFSDCN) is used as the donor of the active layer. The improvement of open-circuit voltage (V_{OC}), short-circuit current (J_{SC}), fill factor (*FF)* are all obtained with an appropriate amount of Au NPs incorporated into the active layer. As a result, after optimization, the improvement of power conversion efficiency (PCE) by ~32% can be achieved. In order to understand the improvement, we will experimentally and theoretically investigate the effects of LSPR introduced by Au NPs on the optical properties of PSCs, particularly the PSC active layer. We will also experimentally and theoretically study the effects of Au NPs on PSC electrical properties. The study therefore contributes to better understanding the uses of Au NPs for enhancing PSC performances.

2. Experimental

2.1 Syntheses of Au NPs and PFSDCN

The syntheses of Au NPs followed the sodium citrate reduction method.[20] After that, 10 mg O-[2-(3-Mercaptopropionylamino)ethyl]-O´-methylpolyethylene glycol (Monofunctional PEG, MW 5000, Sigma-Aldrich) was dissolved in 1 ml de-ionized water, and then the solution was stirred in a rotary evaporator to make it uniform. 0.5 ml Au NPs was added into the solution and then heated at 70°C for 15 minutes to evaporate the water. Then 0.5 ml chloroform/chlorobenzene (1:1 v/v) was added to form well dispersed Au NPs solution. PFSDCN was synthesized via a post-functionalized approach by

treating its aldehyde-contaning precursor polymer, which is prepared by common Suzuki coupling conditions, with malononitrile via Knoevenagel reaction under the presence of pyridine. The procedures were similar to what we reported previously,[21] and the detail information about the synthesis will be reported elsewhere.

2.2 Device fabrication

The fabrication process of PEDOT:PSS (Baytron AI 4083) onto ITO-coated glass substrates can be found elsewhere.[22] Before spin-coating the active layer, polymer blend and Au NPs were mixed in the optimized solvent mixture of chloroform/chlorobenzene (1:1 v/v ratio) to form uniform solution. The final solution consisted of PFSDCN (2 mg/ml) and [6,6]-phenyl-C_{61} butyric acid methyl ester (PCBM, 8 mg/ml, from Nichem Fine Technology Ltd.) and Au NPs with different weight ratio (wt%). The wt% of Au NPs is determined only by considering the weight of PFSDCN. The solution of the polymer blend without Au NPs was also prepared as the control. For the optimized control devices, the mixed solution was spin-coated at 750 rpm for 40 seconds to obtain an active layer with the thickness ~65 nm as determined by stylus profiler. The film was then thermal annealed at 100°C for 10 minutes. Finally, LiF (1 nm)/Al (100 nm) was thermally evaporated as the cathode with a device area of 5.77 mm^2 defined by a shadow mask.

2.3 Device characterization

Transmission Electron Microscope (TEM) images of Au NPs were measured using Philips Tecnai G2 20 S-TWIN. The absolute refractive index and absorption coefficient were measured by Woollam spectroscopic ellipsometry. Current density – voltage (*J*-*V*) measurement can be found elsewhere.[22] The IPCE measurement was performed by a system combining xenon lamp, monochromator, chopper and a lock-in amplifier together with a calibrated silicon photodetector. Atomic force microscope

(AFM) characterization was conducted by using Nanoscope III (Digital Instrument) in the tapping mode.

2.4 Theoretical modelling

In order to investigate the effects of Au NPs on the light absorption at the active layer of PSCs, the light absorption of the active layer, which determines the exciton generation rate, has been theoretically determined. As a rigorous, fast and efficient solver of Maxwell's equation, volume integral equation - Fast Fourier transform (VIE-FFT) has been built in this work. The algorithm is particularly capable of modelling thin-film solar cells incorporating plasmonic NPs of size ranging from 10 nm to 100 nm. The plasmon coupling and hybridization of NPs, as well as their interplay with PSC device structure, have been fully taken into account. We have also theoretically studied the electrical properties of PSCs by solving the organic semiconductor equations involving Poisson, drift-diffusion, and continuity equations.[23,24] Details of the optical and electrical models are described in Supplementary B and C respectively.

3. Results and Discussion

3.1 Overall Experimental Results

The absorption spectrum of PFSDCN film is shown in Fig. 1 and has two absorption peaks at around 374 nm and 518 nm. The chemical structure of PFSDCN is shown in the inset of Fig. 1. The optical bandgap and oxidation potential of PFSDCN are 2.05 eV and 0.91 V, respectively. The highest occupied molecular orbital (HOMO) is -5.32 eV as measured by cyclic voltammetry (CV) method and the lowest unoccupied molecular orbital (LUMO) is -3.27 eV calculated from HOMO level and optical bandgap. The absorption spectrum of Au NPs in chloroform/chlorobenzene (1:1 v/v ratio) is shown in Fig. 2 with the peak at ~ 520 nm. The average diameter of Au NPs is ~18 nm determined from TEM

measurement (inset of Fig. 2). The current density (J) versus voltage (V) characteristics are shown in Fig. 3a. The effects of Au NPs concentration on PSC performances including V_{OC}, J_{SC}, FF and PCE are shown in Fig. 3b (i)-(iv) respectively. It should be noted that the fabrication conditions such as the ratio of PFSDCN to PCBM, spin-coating speed and time, annealing temperature and duration have been optimized for the control devices before the addition of Au NPs.

It is observed that Au NPs with a low concentration of 0.5 wt% improves V_{OC} and J_{SC}. However, both V_{OC} and J_{SC} reduce when Au NPs concentration increases further. FF increases slightly and then decreases as Au NPs concentration increases. From the dark J-V characteristics (Supplementary A: Fig. SA1), the electrical conductivity improves by adding Au NPs, which is in agreement with others reports.[17] The difference here is that the electrical conductivity reduces with the further increase of Au NPs concentration > 2 wt%. Consequently, PCE is improved by ~ 32% from 1.64% (without Au NPs) to 2.17% (with 0.5 wt% Au NPs), and then decreases. When Au NPs concentration reaches 6 wt%, almost no photovoltaic effect is observed (PCE ~ 0.01%).

It should be noted that in the study, Au NPs have been capped with PEG. In order to investigate the effects of PEG on device performances, the PEG-only PSCs were fabricated in which only PEG was incorporated into the polymer blend. PEG concentration in the mixed solution is ~0.08 mg/ml which equals that of the PEG in 0.5 wt% Au NPs mixed with polymer blend solution. As shown in the Supplementary A (Fig. SA2), the PEG-only PSC shows similar J-V characteristics and PCE (~1.67%) to that of the device without PEG incorporation (PCE~1.64%). Therefore, PEG itself is not likely to has pronounced effects on device performances.

3.2 LSPR Effects

To verify the degree of contributions of LSPR effect, we measure the absorption spectrum of the active layer incorporated with various Au NPs concentrations. Meanwhile, to understand the physics, we build a model to rigorously solve Maxwell's equations and study the absorption of PSCs as shown in Fig. 4. The theoretical near-field profile of electric field (Fig. 4b) shows very strong field strength laterally distributed along the active layer which can enhance the light absorption by the polymer blend for generating carriers. It is noteworthy that when Au NPs incorporated into PEDOT:PSS layer (i.e. the layer adjacent to the active layer), the light absorption in the active layer is not clearly enhanced due to the lateral distribution feature of the strong LSPR near field along the PEDOT:PSS layer rather than a vertical distribution into the active layer as described in our another work.[25]

The theoretical and experimental absorption enhancement of the active layer (PFSDCN: PCBM) indicate that LSPR for the case of low Au NPs concentration mixed active layer exists at around 650 nm which is different from that of Au NPs (~ 520 nm) in chloroform/chlorobenzene (1:1 v/v ratio) due to the change of the surrounding optical environment. Moreover, when the spacing between Au NPs reduces (i.e. higher Au NPs concentration), the theoretical and experimental results show that the resonance strength increases and slightly red shifts. Consequently, the theoretical results are in agreement with our experimental results. Our results demonstrate and explain the features of LSPR excited by Au NPs incorporated into PSCs active layer.

The light absorption can be enhanced experimentally by over 100% at the resonance region when Au NPs concentration increases to 6 wt% as shown in Fig. 4a. However, the effects of LSPR alone cannot completely interpret the overall observed phenomena of PSCs. For example, low Au NPs concentration can benefit PSC performances. Continuously enhanced light absorption is obtained with the increase of Au NPs concentration due to the stronger LSPR. However, when Au NPs concentration > 0.5 wt%, deterioration of device performances is obtained, which is quite unexpected in the

viewpoint of LSPR effects. This can be further illustrated from IPCE characteristics as shown in Fig. 5. When the Au NPs concentration reaches 6 wt%, a large absorption enhancement factor is obtained (Fig. 4a), but IPCE decreases to almost zero. Therefore, besides LSPR effects, the effects of Au NPs on PSC electrical properties need to be investigated for understanding the results.

3.3 Effects on Carrier Mobility

Generally, electron and hole mobilities are important factors and should be high enough to guarantee large carrier hopping rate, to avoid carrier recombination and to prevent the build up of space charge.[26,27] For Au NPs incorporated PSCs, we make hole-only and electron-only devices for determining the hole and electron mobility, respectively, by fitting from the dark *J-V* curves using the space-charge limited current (SCLC) model.[28] Hole-only devices have structures of ITO /PEDOT:PSS /polymer blend: Au NPs/Au (20 nm) /Al (80 nm). It has been reported that the work function of ITO can be effectively modified for electron collection in inverted PSCs by evaporating 1 nm of Ca.[29,30] For our electron-only devices, we adopt this method and use the structure of ITO/Ca (2 nm)/polymer blend: Au NPs/LiF(1 nm)/Al(100 nm). The mobility of holes and electrons is shown in Fig. 6 and the detailed experimental data and fitting curves are discussed in Supplementary A (Fig. SA4). The hole mobility ($1.18 \sim 4.25\times10^{-4}$ $cm^2V^{-1}s^{-1}$) is about one order less than electron mobility ($0.78 \sim 1.2\times10^{-3}$ $cm^2V^{-1}s^{-1}$) except for that of PSC with 6 wt% Au NPs (Fig. 6). In addition, the trend of PSC electrical conductivity verse Au NPs concentration (Supplementary A: Fig. SA1) is consistent with that of hole mobility. Hence, the charge transport of our devices is dominantly limited by the hole transport property, which agrees well with the fact that the transport process in the organic materials is dominated by the slow charge carriers.[23]

The effects of Au NPs on the carrier mobility are manifold. On one hand, Au NPs can introduce dopant states within the bandgap of polymer which can provide hopping sites for holes and thus

enhance the mobility.[17] In fact, the metallic NP-induced energy levels for holes have also been reported previously in a hybrid Ag NPs/organic resonant tunneling diode.[31] On the other hand, the incorporated Au NPs will modify the nanoscale morphology of the polymer/fullerene blend, especially with high NPs concentration, which can be evidenced by the AFM image as shown in Fig. 7. The root mean square (RMS) roughness of the active layer increases significantly from ~0.617 nm (without Au NPs) to ~ 8.062 nm (6 wt% Au NPs) and an obvious different surface morphology are observed. In addition, the phase image shows a much larger contrast for the active layer film with 6 wt% Au NPs, indicating a nanoscale morphology change of the blends.[32,33] Such NPs-induced nanoscale morphology change may not favor charge transport and thus degrades the carrier mobility. The two factors will therefore compete with each other in our devices.

At low Au NPs concentration, the blend morphology does not have clear changes from our AFM results (i.e. RMS only increases to ~1.204 nm for 1 wt% Au NP incorporation; figure is not shown here) and therefore only plays a less important role in modifying carrier mobility. As a result, with low Au NPs concentration, the increases of carrier mobility should be explained by the introduction of hopping sites for holes. These hoping sites are expected to have greater influence on hole mobility than electron mobility, which agrees well with the experimental results. Compared with the control devices (without Au NPs), incorporation with 2 wt% Au NPs contributes to an improvement of hole mobility by ~237% (from 1.26×10^{-4} $cm^2V^{-1}s^{-1}$ to 4.25×10^{-4} $cm^2V^{-1}s^{-1}$), and an improvement of electron mobility only by ~28% (from 0.93×10^{-3} $cm^2V^{-1}s^{-1}$ to 1.2×10^{-3} $cm^2V^{-1}s^{-1}$). With high Au NPs concentration, the NP-induced morphology change dominates the charge transport process and thus both the hole and electron mobility are expected to be degraded, which is well consistent with the experimental results as shown in Fig. 6.

Therefore, the enhanced carrier mobilities with the proper amount of Au NPs can partly account for the improved photocurrent generation and *FF* due to the improved carrier collection and the reduced bulk resistance. However, when the carrier mobility maintains increment until Au NPs concentration reaching 2 wt%, device performances, i.e. J_{SC} and PCE decrease when Au NPs concentration ≥1 wt%. This indicates that besides the carrier mobility, Au NPs should affect other operation processes of PSCs. One process likely to be affected is the dissociation of excitons to free carriers as described below.

3.4 Effects on Exciton Dissociation

To investigate the efficiency of exciton dissociation, photocurrent (J_{ph}) as a function of effective voltage (V_{EFF}) is measured and fitted following Mihailetchi et al.[34] The $J_{ph} \sim V_{EFF}$ features and the corresponding fitting curves are shown in Supplementary A: Fig. SA5. The maximal generation rate of excitons (G_{max}) for all the samples is obtained to be on the order of 5×10^{27} m^{-3} s^{-1}. The exciton decay rate (k_F) and exciton dissociation probability (P_{exc}) under short-circuit condition are shown in Fig. 8. It can be observed that Au NPs indeed affects the exciton dissociation. Low Au NPs concentration makes k_F reduce and P_{exc} increase slightly from ~76% to ~80%. While Au NPs concentration further increases, P_{exc} reduces.

The slight enhancement of P_{exc} at low Au NPs concentration can be attributed to the excitation of LSPR[14] and the enhanced hole mobility which reduces the carrier back-transfer induced recombination.[23,26] The degradation of exciton dissociation efficiency at high NPs concentration can be attributed to the polymer morphology change. The morphology change has two effects: bulk and interfacial effects. The bulk effect is the NPs-induced nanoscale morphology change inside the active layer, which is significant especially at high NPs concentration as described above and shown in Fig. 7. The morphology change may make the polymer blend less favorable for exciton dissociation. The interfacial effect is also known as the segregation effect.[19] The aggregation of Au NPs at the interface

between organic active layer and cathode will break down the Fermi level pinning and downward shift the work function of the cathode, and thus reduces the built-in potential and $V_{OC.}$ In our results, the segregation effect can be indicated by the reduction of V_{OC} for the devices with Au NPs concentration ≥ 1 wt% as shown in Fig. 3b(i). The decrease of built-in electric field in the active layer would make the exciton dissociation process less efficient since the exciton dissociation is very field-dependent.[5] The aggregation of NPs can be clearly observed from the surface morphology of the active layer with 6 wt% Au NPs as shown in Fig. 7, which thus degrade our device performances.

3.5 V_{OC}

As Au NPs concentration increases, V_{OC} first increases from ~0.90 V (without Au NPs) to ~1.01 V (Au NPs: 0.5 wt%) and then decreases. When Au NPs concentration increases to 6 wt%, V_{OC} reduces significantly to 0.44 V. In BHJ PSCs, charge recombination is commonly regarded as one important loss mechanism limiting V_{OC}.[35,36] With a proper amount of Au NPs (≤ 0.5%), the reduced recombination due to the enhanced carrier mobility and exciton dissociation is expected to improve V_{OC}. To understand the contribution of recombination reduction on V_{OC}, a theoretical model is built based on the fundamental equations describing carrier transports in semiconductors following Koster et al.[23] Details of the model can be found in Supplementary C. In modeling, the device parameters for PSCs with various Au NPs such as carrier mobilities and k_F are obtained from Part 3.3 and 3.4 above while other parameters are remained constant. The results show that V_{OC} has almost no change, suggesting that the reduced recombination due to increased carrier mobilities does not contribute to the V_{OC} improvement. An alternative explanation for the V_{OC} improvement with Au NPs incorporation (≤ 0.5 wt%) is the downwards shift of the donor HOMO level due to reduced polarization energy.[37,38] Downwards shift of donor HOMO level by 0.1 eV is best fitted as shown in Supplementary C: Fig. SC1, for the increase of the measured V_{OC} by ~ 0.1V for 0.5 wt% Au NP case.

The degradation of V_{OC} at high Au NPs concentration is due to several factors. At high Au NPs concentration, Au NP aggregation as stated in Part 3.4 becomes severe as shown in Fig. 7 which contributes to the V_{OC} reduction. When the segregation effect induces a blocking contact at the cathode, V_{OC} will significantly reduce. Our theoretical results show that the change of work function of the cathode causes the reduction of V_{OC}. When the cathode work function is downward shifting by 0.56 eV, V_{OC} reduces to 0.69 V for PSCs with 4 wt% of Au NPs concentration (Fig. SC1). The other subordinate factor resulting in V_{OC} reduction is that more shunt paths are induced by the Au NPs, which can be well indicated from the increased reverse current for the PSCs as the concentration of Au NPs increases (see Supplementary A: Fig. SA1). The shunt paths formed directly from anode to cathode are believed to reduce the V_{OC}.[39,40]

4. Conclusions

In this study, the effects of monofunctional PEG-capped Au NPs (0.5 wt%) on PSCs have been theoretically and experimentally investigated by introducing the Au NPs into the blend of newly synthesized polymer of PFSDCN and PCBM. Our results show that due to the interesting feature of the strong lateral distribution of LSPR near field along the active layer, light absorption is enhanced by incorporating Au NPs into the active layer. The understanding can be applied to other metallic NPs incorporated organic solar cells. Meanwhile, our results show that electrical properties can counter-diminish the optical enhancement from LSPR which reduces the overall performance improvement. It is important that both optical and electrical properties need to be studied and optimized simultaneously. Our results show that after optimization, power conversion efficiency can be improved by ~32%. The study contributes to better understanding the uses of Au NPs for enhancing PSC performances.

Acknowledgements

This work is supported UGC grant (#400897) of the University of Hong Kong and Hong Kong Research Grants Council (HKU#712108 and HKU#712010) from the Research Grants Council of the HK Special Administrative Region, China. Huang would like to acknowledge the financial support from the Natural Science Foundation of China (No. 50990065, 51010003, 51073058 and 20904011), the Ministry of Science and Technology, China (MOST) National Research Project (No. 2009CB623601) and the Fundamental Research Funds for the Central Universities, South China University of Technology (No.2009220012).

Figures

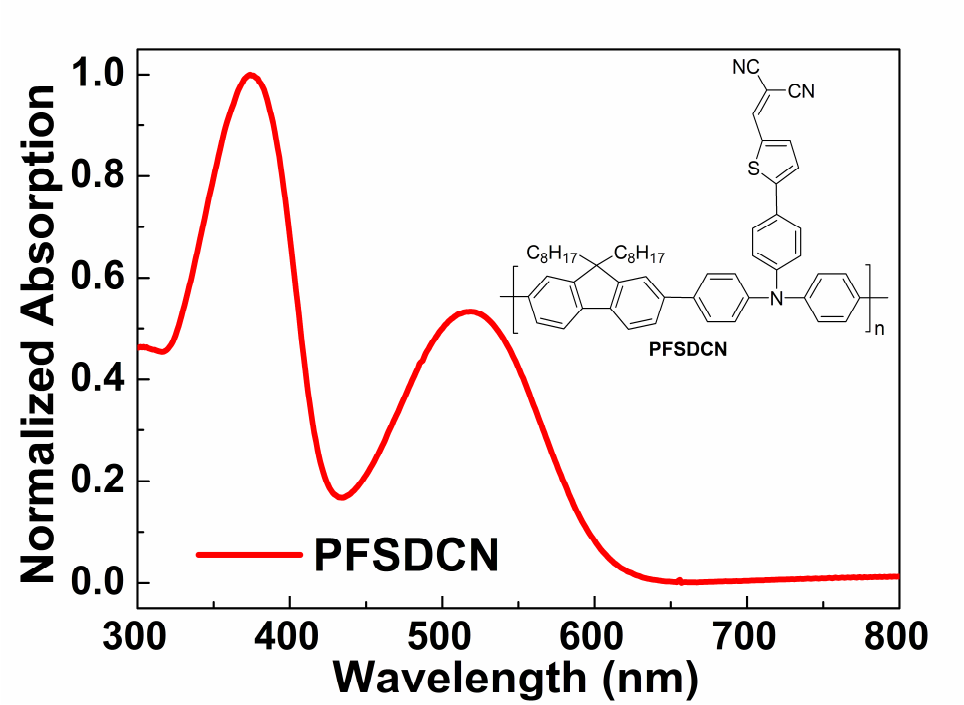

Fig. 1 The normalized absorption spectrum and chemical structure of PFSDCN.

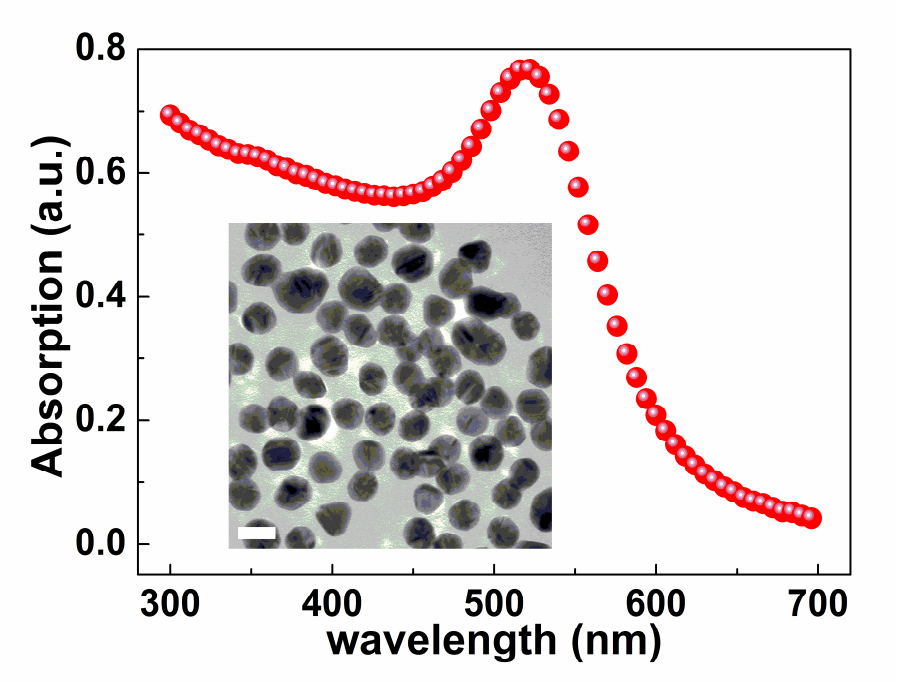

Fig. 2 The absorption spectrum of Au NPs in chloroform/chlorobenzene (1:1 volume ratio) with the peak at ~ 520 nm. Inset is the TEM image of Au NPs. The white colour bar is 20 nm long.

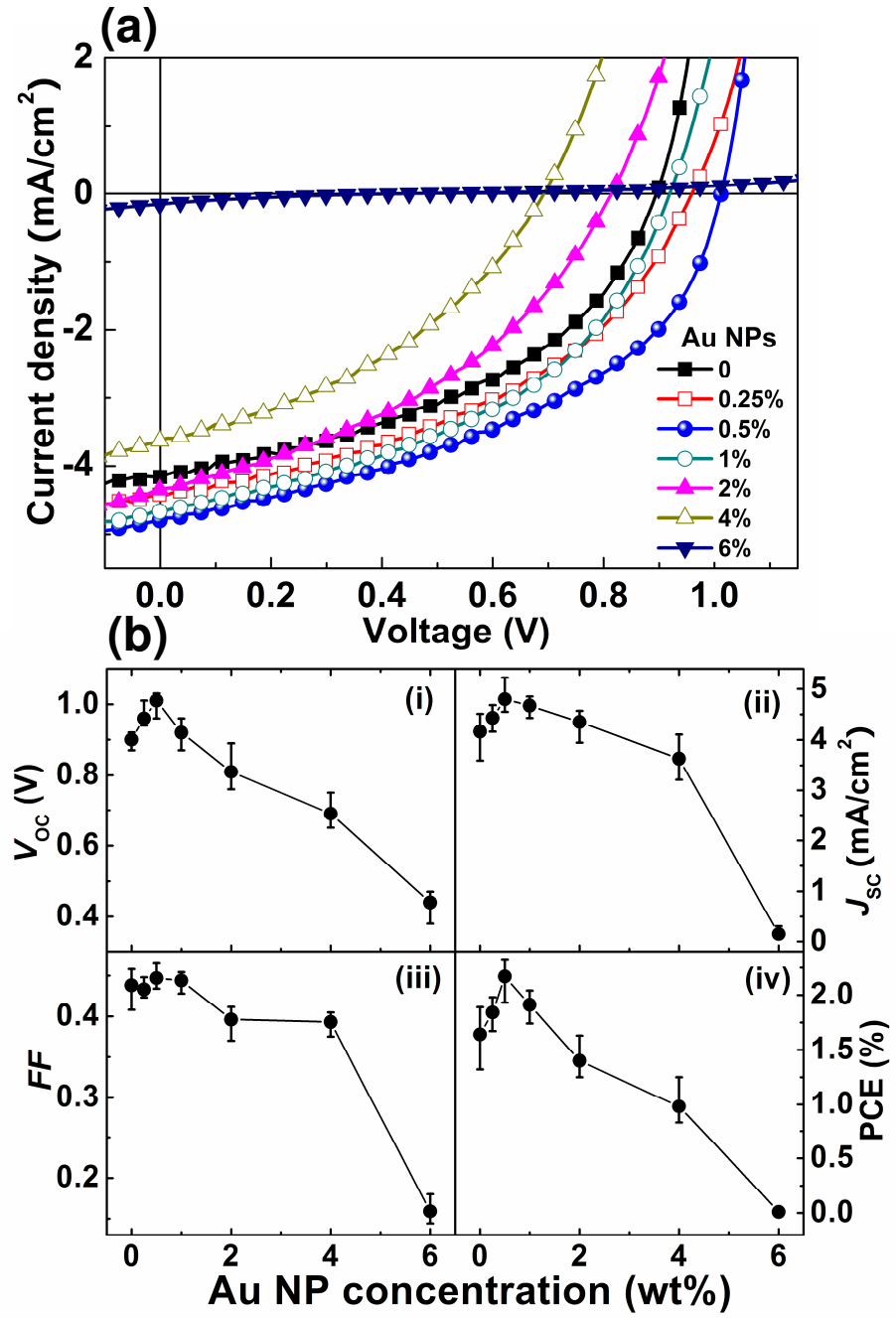

Fig. 3 (a) The current-voltage characteristics of the representative PSCs incorporated with different NP concentration under AM 1.5G illumination at 100 mW/cm^2.(b) Electrical parameters of NP incorporated PSCs: (i) V_{OC}; (ii) J_{SC}; (iii) *FF*; (iv) PCE.

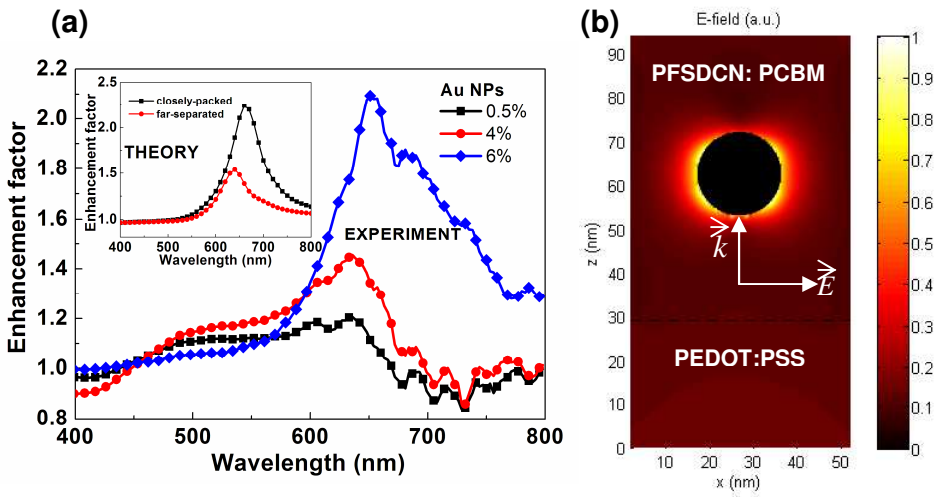

Fig. 4 (a) Experimental and theoretical (inset) absorbance enhancement factor of the active layer with different amount of Au NPs. (b) Theoretical near field distribution around an Au NP in the active layer.

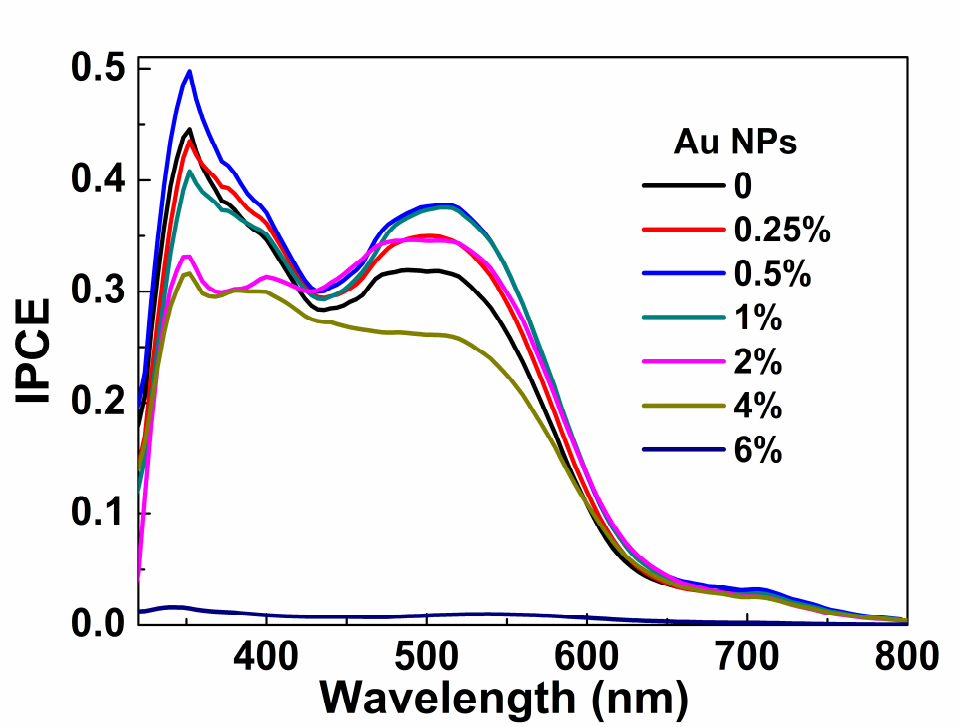

Fig. 5 IPCE of PSCs incorporated with different concentrations of Au NPs.

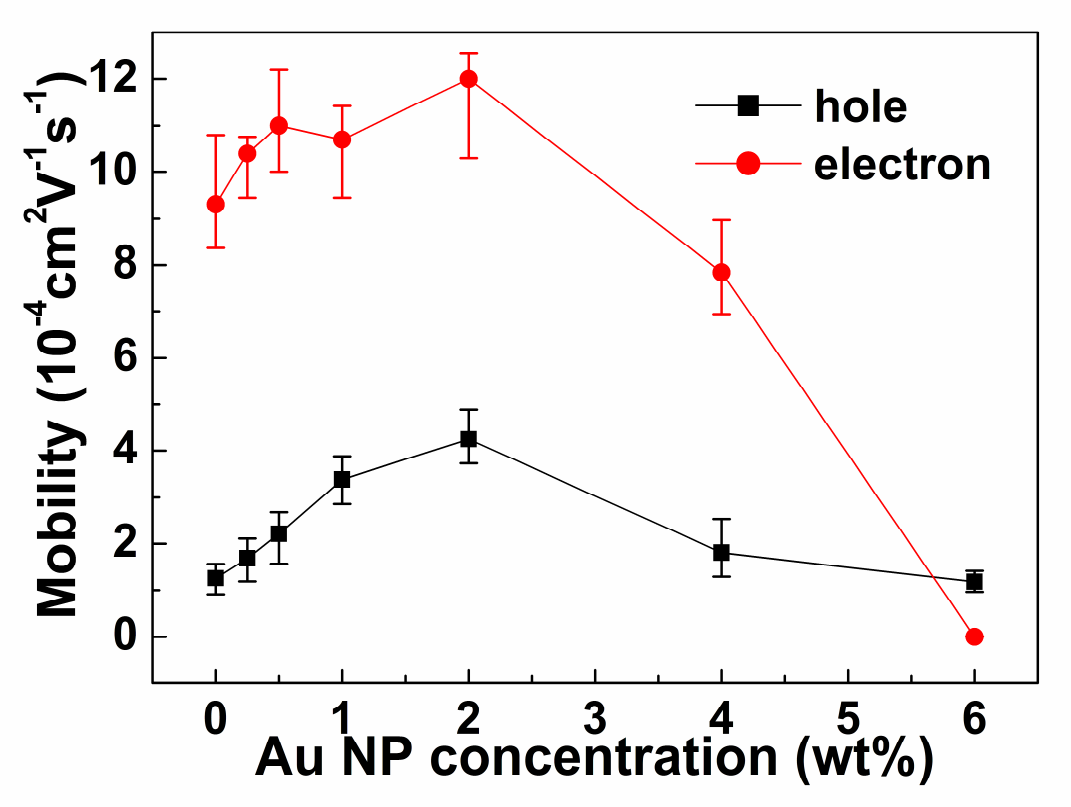

Fig. 6 Effects of Au NP concentration on the hole and electron mobilities in the active layer**.**

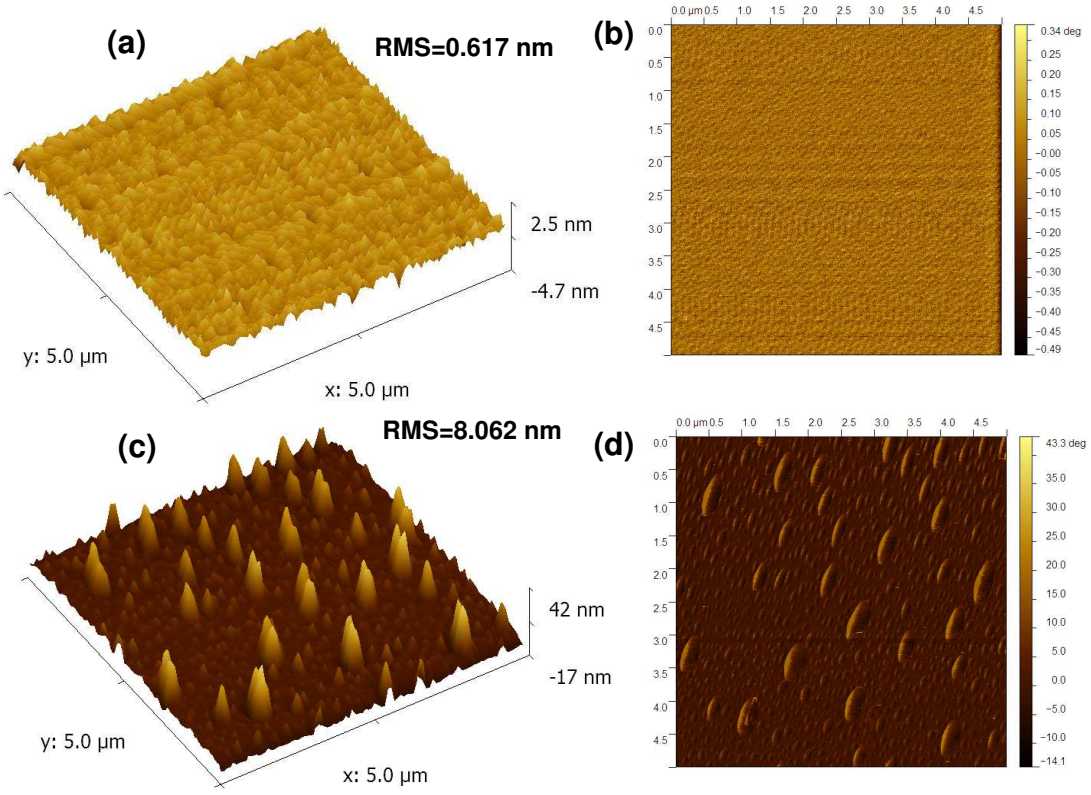

Fig. 7 AFM images of the active layer (a) height image, RMS=0.617 nm and (b) phase image of active layer film without Au NPs; (c) height image, RMS=8.062 nm and (b) phase image of active layer film with Au NPs: 6 wt%.

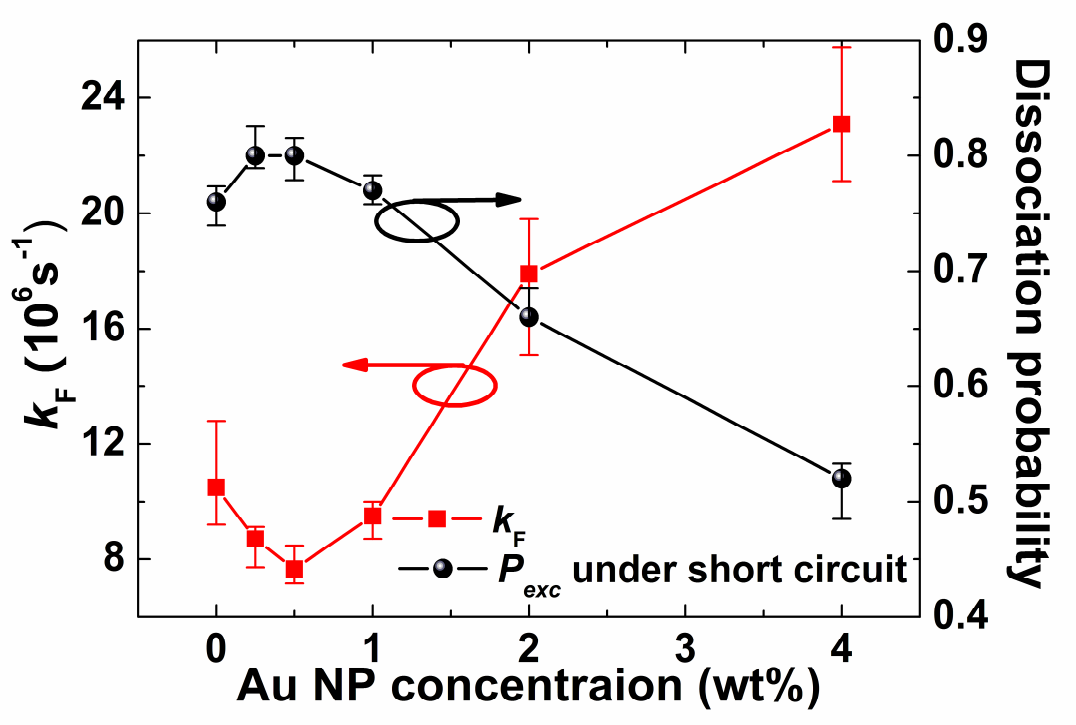

Fig. 8 Effects of Au NP concentration on the decay rate of bound electron-hole pair (k_F) (square) and exciton dissociation probability (P_{exc}) under short circuit condition (circle).

References

1 G. Yu, J. Gao, J. C. Hummelen, F. Wudl and A. J. Heeger, *Science*, 1995, **270**, 1789.

2 C. J. Brabec, G. Zerza, G. Cerullo, S. De Silvestri, S. Luzzati, J. C. Hummelen and S. Sariciftci, *Chem. Phys. Lett.*, 2001, **340**, 232.

3 D. Wöhrle and D. Meissner, *Adv. Mater.*, 1991, **3**, 129.

4 V. Shrotriya, E. H. -E. Wu, G. Li, Y. Yao and Y. Yang, *Appl. Phys. Lett.*, 2006, **88,** 064104.

5 P. W. M. Blom, V. D. Mihailetchi, L. J. A. Koster and D. E. Markov, *Adv. Mater.*, 2007, **19,** 1551.

6 H. A. Atwater and A. Polman, *Nat. Mater.*, 2010, **9**, 205.

7 J. R. Cole and N. J. Halas, *Appl. Phys. Lett.*, 2006, **89**, 153120.

8 S. -S. Kim, S. -I. Na, J. Jo, D. -Y. Kim and Y. -C. Nah, *Appl. Phys. Lett.*, 2008, **93**, 073307.

9 C. Min, J. Li, G. Veronis, J. -Y. Lee, S. Fan and P. Peumans, *Appl. Phys. Lett.*, 2010, **96**, 133302.

10 W. E. I. Sha, W. C. H. Choy and W. C. Chew, *Opt. Lett.*, 2011, **36**, 478.

11 W. E. I. Sha, W. C. H. Choy and W. C. Chew, *Opt. Express*, 2010, **18**, 5993.

12 Y. A. Akimov, W. S. Koh, S. Y. Sian and S. Ren, *Appl. Phys. Lett.*, 2010, **96**, 073111.

13 J. -L. Wu, F. -C. Chen, Y. -S. Hsiao, F. -C. Chien, P. Chen, C. -H. Kuo, M. H. Huang and C. -S. Hsu, *ACS Nano*, 2011, **5**, 959.

14 F. -C. Chen, J. -L. Wu, C. -L. Lee, Y. Hong, C. -H. Kuo and M. H. Huang, *Appl. Phys. Lett.*, 2009**, 95**, 013305.

15 A. J. Morfa, K. L. Rowlen, T. H. Reilly, Iii, M. J. Romero and J. van de Lagemaat, *Appl. Phys. Lett.*, 2008, **92**, 013504.

16 W. -J. Yoon, K. -Y. Jung, J. Liu, T. Duraisamy, R. Revur, F. L. Teixeira, S. Sengupta and P. R. Berger, *Sol. Energy Mater. Sol. Cells*, 2010, **94**, 128.

17 K. Kim and D. L. Carroll, *Appl. Phys. Lett.*, 2005, **87**, 203113.

18 B. V. K. Naidu, J. S. Park, S. C. Kim, S. -M. Park, E. -J. Lee, K. -J. Yoon, S. J. Lee, J. W. Lee, Y. -S. Gal and S. -H. Jin, *Sol. Energy Mater. Sol. Cells*, 2008, **92**, 397.

19 K. Topp, H. Borchert, F. Johnen, A. V. Tunc, M. Knipper, E. von Hauff, J. Parisi and K. Al-Shamery, *J. Phys. Chem. A*, 2009, **114**, 3981.

20 S. Link and M. A. El-Sayed, *J. Phys. Chem. B*, 1999, **103**, 4212.

21 C. Duan, W. Cai, F. Huang, J. Zhang, M. Wang, T. Yang, C. Zhong, X. Gong and Y. Cao, *Macromolecules*, 2010, **43**, 5262.

22 C.-D. Wang and W. C. H. Choy, *Sol. Energy Mater. Sol. Cell*, 2011, **95**, 904.

23 L. J. A. Koster, E. C. P. Smits, V. D. Mihailetchi and P. W. M. Blom, *Phys. Rev. B*, 2005, **72**, 085205.

24 D. W. Sievers, V. Shrotriya and Y. Yang, *J. Appl. Phys.*, 2006, **100**, 114509.

25 Dixon D.S. Fung, L. Qiao, W. C.H. Choy, C.-D. Wang, W. E.I. Sha, F.-X. Xie and S. He, *J. Mater. Chem.*, DOI:10.1039/C1JM12820E

26 A. C. Mayer, S. R. Scully, B. E. Hardin, M. W. Rowell and M. D. McGehee, *Mater. Today*, 2007, **10**, 28.

27 M. M. Mandoc, L. J. A. Koster and P. W. M. Blom, *Appl. Phys. Lett.*, 2007, **90**, 133504.

28 V. D. Mihailetchi, J. K. J. van Duren, P. W. M. Blom, J. C. Hummelen, R. A. J. Janssen, J. M. Kroon, M. T. Rispens, W. J. H. Verhees and M. M. Wienk, *Adv. Funct. Mater.*, 2003, **13**, 43.

29 D. W. Zhao, P. Liu, X. W. Sun, S. T. Tan, L. Ke and A. K. K. Kyaw, *Appl. Phys. Lett.* 2009**,** **95**, 153304.

30 C. Y. Jiang, X. W. Sun, D. W. Zhao, A. K. K. Kyaw and Y. N. Li, *Sol. Energy Mater. Sol. Cells*, 2010, **94**, 1618.

31 T. Zheng, W. C. H. Choy and Y. Sun, *Adv. Funct. Mater.*, 2009, **19**, 2648.

32 H. -Y. Chen, J. Hou, S. Zhang, Y. Liang, G. Yang, Y. Yang, L. Yu, Y. Wu and G. Li, *Nat. Photon.*, 2009, **3**, 649.

33 Z. Xu, L. -M. Chen, G. Yang, C. -H. Huang, J. Hou, Y. Wu, G. Li, C. -S. Hsu and Y. Yang, *Adv. Funct. Mater.*, 2009, **19**, 1227.

34 V. D. Mihailetchi, L. J. A. Koster, J. C. Hummelen and P. W. M. Blom, *Phys. Rev. Lett.*, 2004, **93**, 216601.

35 C. J. Brabec, A. Cravino, D. Meissner, N. S. Sariciftci, T. Fromherz, M. T. Rispens, L. Sanchez and J. C. Hummelen, *Adv. Funct. Mater.*, 2001, **11**, 374.

36 K. Vandewal, K. Tvingstedt, A. Gadisa, O. Inganas and J. V. Manca, *Nat. Mater.*, 2009, **8**, 904.

37 K. Akaike, K. Kanai, Y. Ouchi and K. Seki, *Adv. Funct. Mater.*, **2010**, *20*, 715.

38 W. Tress, K. Leo and M. Riede, *Adv. Funct. Mater.*, 2011, **21**, 2140.

39 H. J. Snaith, N. C. Greenham and R. H. Friend, *Adv. Mater.*, 2004, **16**, 1640.

40 B. Sun, H. J. Snaith, A. S. Dhoot, S. Westenhoff and N. C. Greenham, *J. Appl. Phys.*, 2005, **97**, 014914.

Supporting Information

Optical and Electrical Effects of Gold Nanoparticles in the active layer of Polymer Solar Cells

Charlie C. D. Wang[a], Wallace C. H. Choy[a]*, Chunhui Duan[b], Dixon D. S. Fung[a], Wei E.I. Sha[a], Feng-xian Xie[a], Fei Huang[b]*, and Yong Cao[b]

[a]Department of Electrical and Electronic Engineering, University of Hong Kong, Pokfulam Road, Hong Kong, China.

[b]Institute of Polymer Optoelectronic Materials & Devices, State Key Laboratory of Physics and Chemistry of Luminescence, South China University of Technology, Guangzhou 510640, P. R. China

* to whom correspondence should be addressed: email: chchoy@eee.hku.hk; Tel: (852)-28578485, Fax: (852) 2559-8738; msfhuang@scut.edu.cn, Tel: (86)-20-8711-4346.

Supplementary A

Supplementary Figures

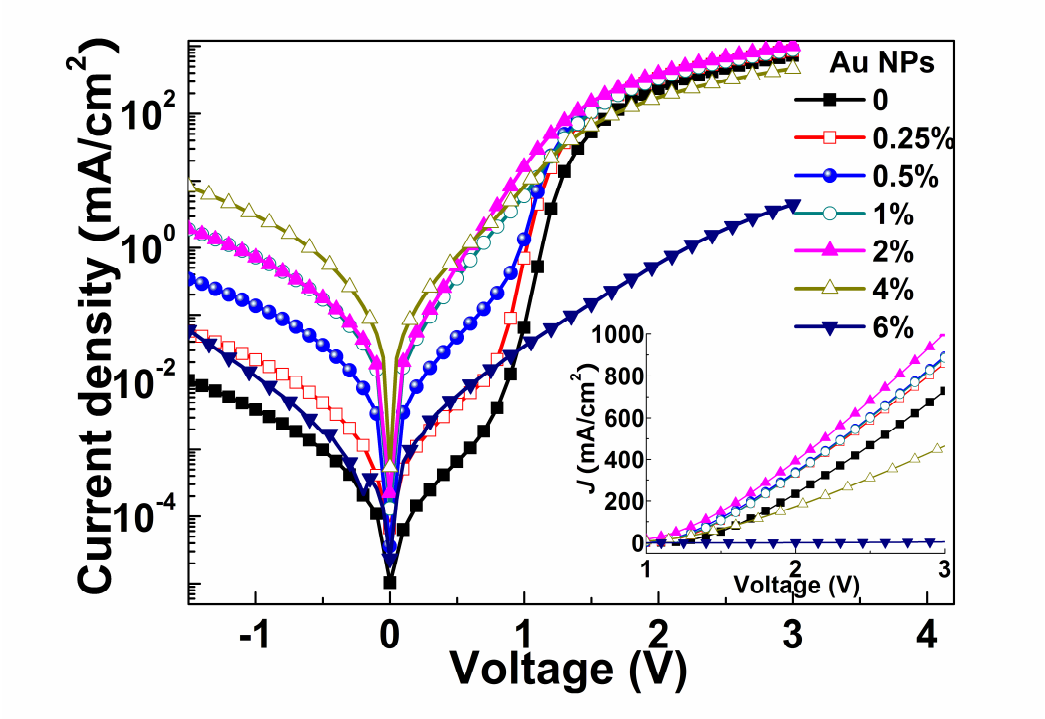

Fig. SA1 The dark current-voltage characteristics of the representative Au NP incorporated PSCs.

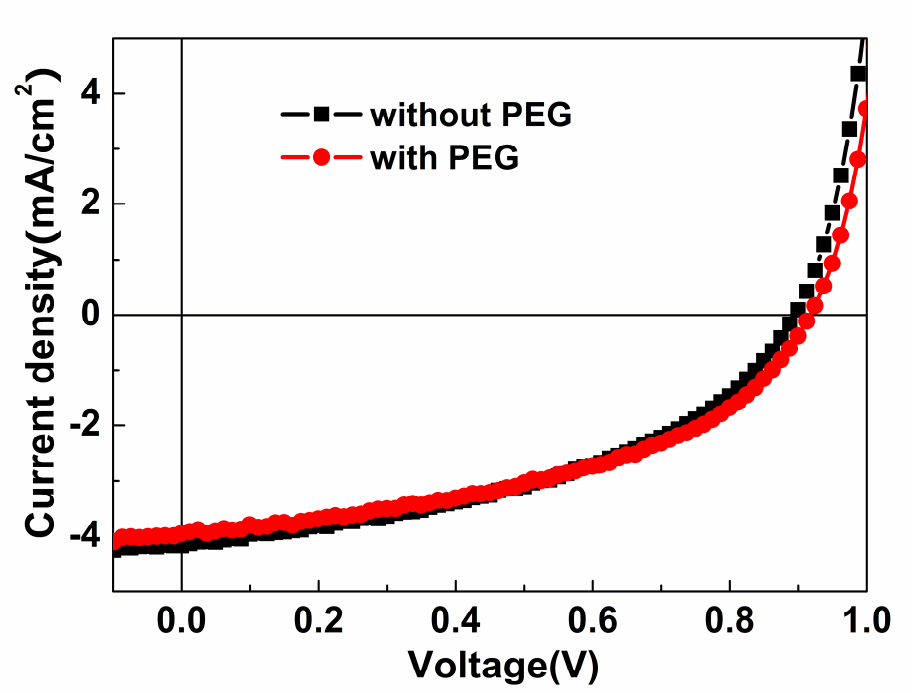

Fig. SA2 The effect of PEG on the current-voltage characteristics of PSCs.

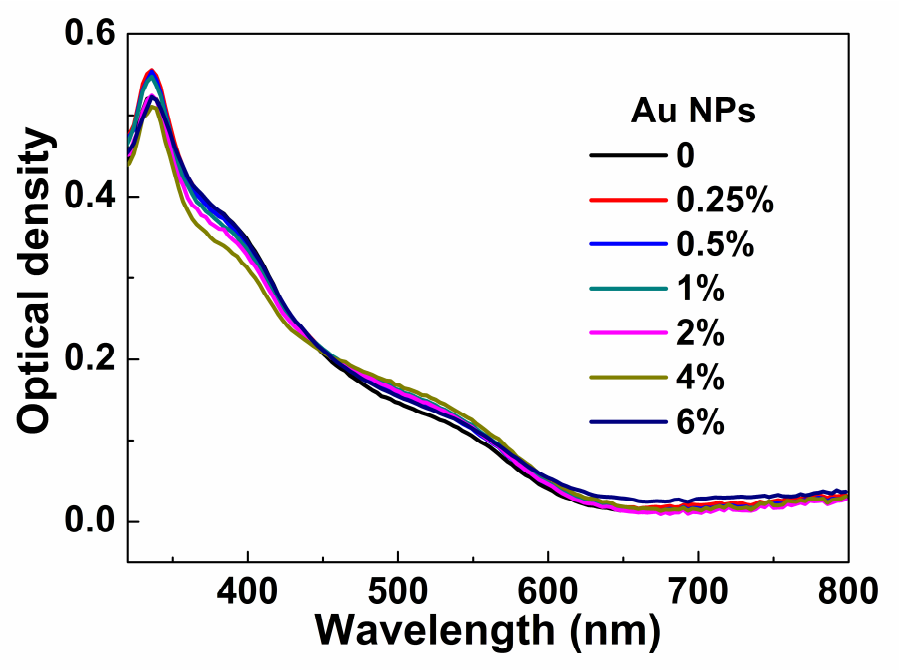

Fig. SA3 The optical densities for the PSCs incorporated with different Au NP concentrations.

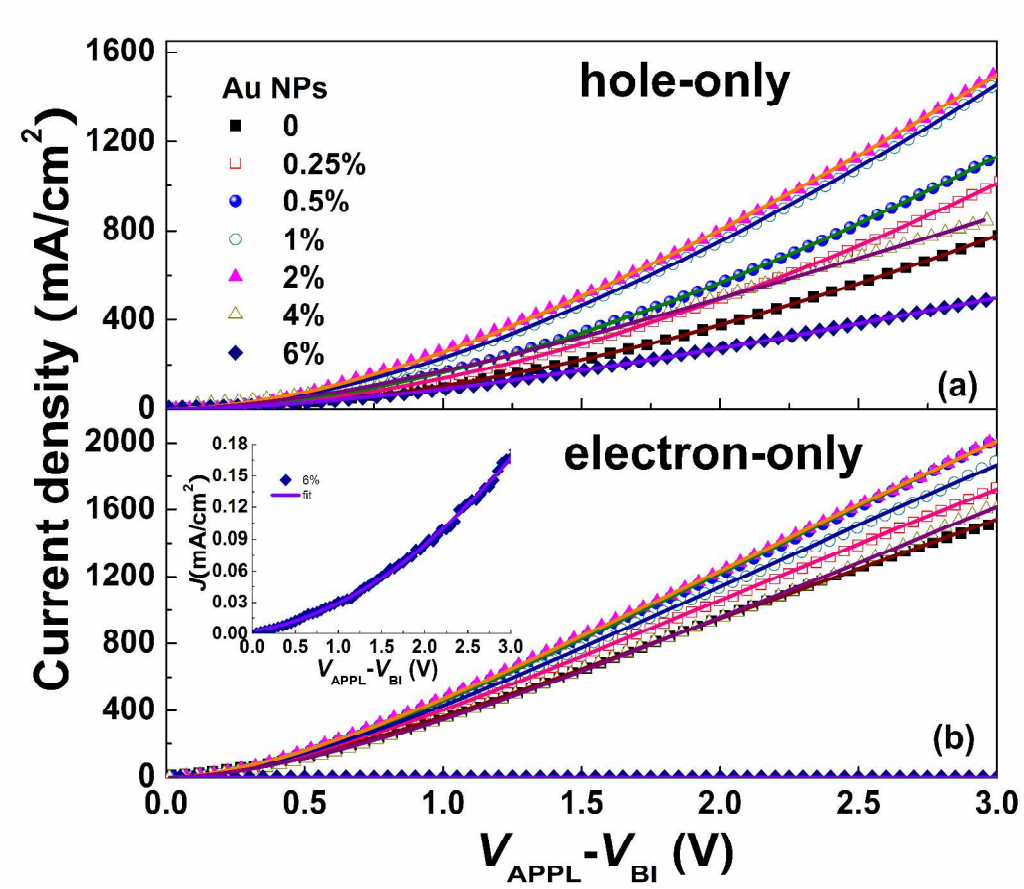

Fig. SA4 Experimental data (symbols) and fitted *J-V* curves (solid lines) of (a) hole-only devices (b) electron-only devices. The electrical conductivity of electron-only device with 6 wt% Au NP concentration is rather low and thus is shown in the inset of (b).

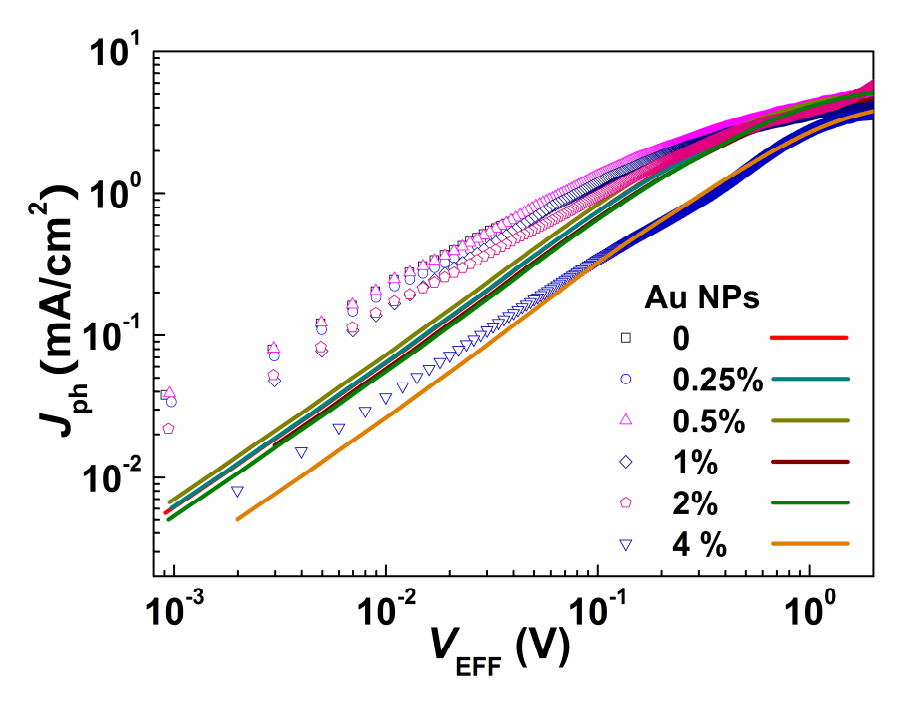

Fig. SA5 Experimental data (symbols) and fitted curves (solid lines) of photocurrent versus effective voltage for PSCs incorporated with different Au NP concentrations.

Supplementary B

In order to understand the detail physics of plasmonic effects of Au NPs on PSCs, we build an efficiency model to rigorously solve Maxwell's equations. We adopt the fast algorithm of volume integral equation - Fast Fourier transform (VIE-FFT) to solve Maxwell's equations. Details of the model are described as below.

1 Volume Integral Equation Method

The scattered electric field generated by the volumetric polarization current $\mathbf{J}$ can be written as

$$\mathbf{E}^s(\mathbf{r}) = -j_0\omega\mu_0\int_v \overline{\mathbf{G}}(\mathbf{r},\mathbf{r}')\cdot\mathbf{J}(\mathbf{r}')d\mathbf{r}' \tag{1}$$

where ω is the angular frequency, and $\overline{\mathbf{G}}(\mathbf{r},\mathbf{r}')$ is the dyadic Green's function given by

$$\overline{\mathbf{G}}(\mathbf{r},\mathbf{r}') = \left(\bar{\mathbf{I}} + \frac{\nabla\nabla}{k_0^2}\right)g(\mathbf{r},\mathbf{r}'), g(\mathbf{r},\mathbf{r}') = \frac{\exp\left(-jk_0|\mathbf{r}-\mathbf{r}'|\right)}{4\pi|\mathbf{r}-\mathbf{r}'|} \tag{2}$$

where k_0 is the wavenumber of free space. For the non-magnetic optical materials ($\mu_r = 1$), the volume integral equation (VIE) is of form

$$\mathbf{E}^i(\mathbf{r}) = \frac{\mathbf{J}(\mathbf{r})}{j_0\omega\left(\varepsilon(\mathbf{r})-\varepsilon_0\right)} - \mathbf{E}^s(\mathbf{r}) \tag{3}$$

where $\varepsilon(\mathbf{r})$ is the position-dependent permittivity of the inhomogeneous materials, and $\mathbf{E}^i(\mathbf{r})$ is the incident electric field.

Considering the Cartesian coordinate system, we use the short notation (u_1,u_2,u_3) substituting for (x,y,z), then we have

$$\begin{bmatrix} E_1^s \\ E_2^s \\ E_3^s \end{bmatrix} = \begin{bmatrix} L_{11} & L_{12} & L_{13} \\ L_{21} & L_{22} & L_{23} \\ L_{31} & L_{32} & L_{33} \end{bmatrix}\begin{bmatrix} J_1 \\ J_2 \\ J_3 \end{bmatrix} \tag{4}$$

where

$$L_{ij} = \begin{cases} L_{ii}^c + L_{ii}^q, i = j \\ L_{ij}^q, i \neq j \end{cases} \tag{5}$$

$$L_{ii}^{c} J_i = -j_0 \omega \mu_0 \int_v g(\mathbf{r}, \mathbf{r}') J_i(\mathbf{r}') d\mathbf{r}' \tag{6}$$

$$L_{ij}^{q} J_j = \frac{-j_0}{\omega \varepsilon_0} \frac{\partial}{\partial u_i} \int_v g(\mathbf{r}, \mathbf{r}') \frac{\partial J_j(\mathbf{r}')}{\partial u_j'} d\mathbf{r}' \tag{7}$$

Using the rooftop basis functions to expand the unknown currents, we have

$$\mathbf{J}(\mathbf{r}) = \sum_{i=1}^{3} \mathbf{u}_i \sum_{k,m,n} J_i^D(k,m,n) T_{k,m,n}^i \tag{8}$$

where $T_{k,m,n}^1$, $T_{k,m,n}^2$, and $T_{k,m,n}^3$ are the volumetric rooftop functions given by

$$\begin{aligned} T_{k,m,n}^1 &= \Lambda_k(u_1)\Pi_m(u_2)\Pi_n(u_3) \\ T_{k,m,n}^2 &= \Pi_k(u_1)\Lambda_m(u_2)\Pi_n(u_3) \\ T_{k,m,n}^3 &= \Pi_k(u_1)\Pi_m(u_2)\Lambda_n(u_3) \end{aligned} \tag{9}$$

The functions $\Lambda_k(u_1)$ and $\Pi_m(u_2)$ are defined by

$$\begin{aligned} \Lambda_k(u_1) &= \begin{cases} 1 - \dfrac{|u_1 - k\Delta u_1|}{\Delta u_1}, |u_1 - k\Delta u_1| \le \Delta u_1 \\ 0, \text{else} \end{cases} \\ \Pi_m(u_2) &= \begin{cases} 1, \left| u_2 - \left(m - \dfrac{1}{2} \right) \Delta u_2 \right| < \dfrac{\Delta u_2}{2} \\ 0, \text{else} \end{cases} \end{aligned} \tag{10}$$

The cuboid cells are employed to discretize the structure to be modeled. Here, Δu_1 and Δu_2 are the grid sizes of each small cuboid along x and y directions, respectively. Other functions in (9) can be defined as the same way.

As a result, the discretized form for the operator L_{ii}^{c} in (6) can be written as

$$L_{ii}^{D,c} J_i^D = -j_0 \omega \mu_0 g^D \otimes J_i^D \tag{11}$$

where $\otimes$ denotes the discrete convolution

$$g^D \otimes J_i^D = \sum_{k,m,n} g^D(k-k', m-m', n-n') J_i^D(k', m', n') \tag{12}$$

and

$$g^D(k,m,n)=\int_0^{\Delta u_1}\int_0^{\Delta u_2}\int_0^{\Delta u_3} g(u_{1,k}-u_1',u_{2,m}-u_2',u_{3,n}-u_3')du_{1'}du_{2'}du_{3'} \tag{13}$$

Likewise, the operator $L_{12}^{D,q}$ in (7) can be discretized as

$$\begin{aligned} L_{12}^{D,q}J_2^D &= \frac{-j_0}{\omega\varepsilon_0\Delta u_1\Delta u_2}\left[g^D(k+1,m,n)-g^D(k,m,n)\right] \\ &\otimes\left[J_2^D(k,m,n)-J_2^D(k,m-1,n)\right] \\ &= \frac{-j_0}{\omega\varepsilon_0\Delta u_1\Delta u_2}\left\{\left[g^D(k+1,m,n)-g^D(k,m,n)\right]\right. \\ &\left.-\left[g^D(k+1,m-1,n)-g^D(k,m-1,n)\right]\right\}\otimes J_2^D(k,m,n) \end{aligned} \tag{14}$$

where the finite-difference method is used for the smooth approximation of the dyadic Green's function.

The computations of the discrete convolutions can be performed efficiently by means of cyclic convolutions and fast Fourier transform (FFT), which is similar to the discrete dipole approximation (DDA) method.

2 The Biconjugate Gradient Stabilized Algorithm

The resulting VIE matrix equation can be expressed as

$$Ax=b$$

The procedure of the biconjugate gradient stabilized (BI-CGSTAB) algorithm is given as follows:

Give an initial guess x_0, we have

$$\begin{aligned} &r_0=b-Ax_0,\hat{r}_0=r_0 \\ &\rho_0=\alpha=\omega_0=1 \\ &v_0=p_0=0 \end{aligned}$$

Iterate for $i=1,2,\cdots,n$

$$\rho_i = \langle \hat{r}_0, r_{i-1} \rangle$$
$$\beta = (\rho_i / \rho_{i-1})(\alpha / \omega_{i-1})$$
$$p_i = r_{i-1} + \beta(p_{i-1} - \omega_{i-1} v_{i-1})$$
$$v_i = A p_i$$
$$\alpha = \rho_i / \langle \hat{r}_0, v_i \rangle$$
$$s = r_{i-1} - \alpha v_i$$
$$t = As$$
$$\omega_i = \langle t, s \rangle / \langle t, t \rangle$$
$$x_i = x_{i-1} + \alpha p_i + \omega_i s$$
$$r_i = s - \omega_i t$$

Terminate when

$$\frac{\| r_i \|_2}{\| b \|_2} < \eta$$

where η is the tolerance that specifies the desired accuracy of solution.

Supplementary C

The electrical properties of PSCs have been theoretically studied by solving the organic semiconductor equations involving Poisson, drift-diffusion, and continuity equations [refer to: Mihailetchi et al. Phys. Rev. Lett. 93, 216601 (2004); Koster et al. Phys. Rev. B 72, 085205 (2005); Sievers et al. J. Appl. Phys. 100, 114509 (2006)]. The field dependent mobility uses the Frenkel-Poole form $\mu=\mu_0\exp(F/F_0)$. The Braun-Onsager model is employed for the exciton dissociation. The boundary conditions for ohmic or schottky contacts are also taken into account.

Due to the very thin active layer (~ 65 nm), it can be assumed the generation rate of bound electron-hole pairs (G_{max}) is uniform. G_{max} can be obtained from the measured absorption spectra. The electron and hole mobilities can be obtained by fitting the *J-V* curves of the measured electron- and hole-only devices following the space-charge limited current (SCLC) model. The highest occupied molecular orbital (HOMO) is -5.32 eV as measured by cyclic voltammetry (CV) method and the lowest unoccupied molecular orbital (LUMO) is **-**3.27 eV calculated from HOMO level and optical bandgap. The exciton decay rate (k_F) of exciton and charge separation distance (a) can be fitted to make our theoretical *J-V* curves best fit to the experimental *J-V* curves. The detailed analysis can be referred to "Results and discuss: Part 3.5" in the manuscript.

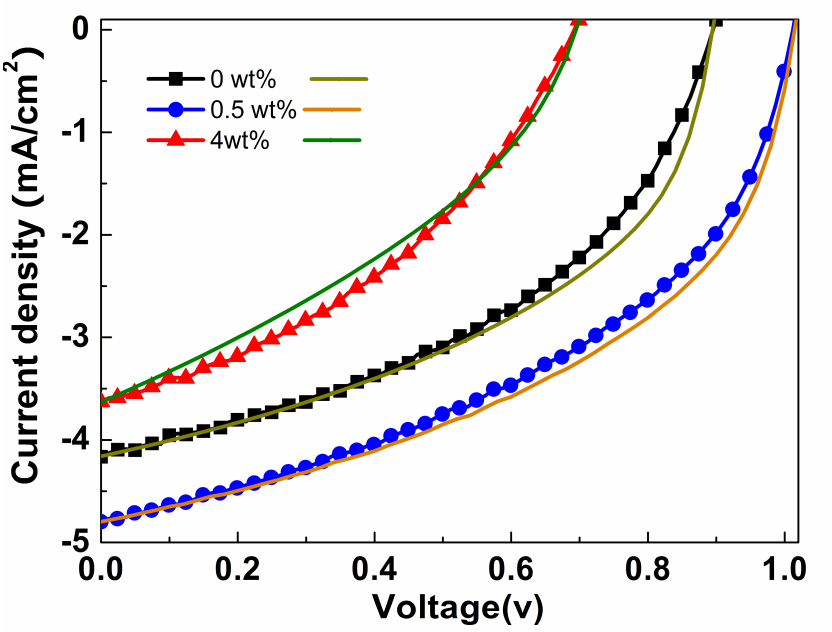

Fig. SC1 *J-V* characteristics of the PSCs with different Au NPs concentration under AM 1.5G illumination at 100 mW/cm^2. The symbols denote experimental data (squares: without Au NPs; circles: Au NPs 0.5 wt%; triangles: Au NPs 4 wt%). The solid lines denote theoretical results.